THE JOURNAL OF PHYSICAL CHEMISTRY A
A JOURNAL OF THE AMERICAN CHEMICAL SOCIETY

pubs.acs.org/JPCA

Article

Autoxidation Mechanism and Kinetics of Methacrolein in the Atmosphere

Zhaoyan Zhang, Chong Wang, Yingqi Zhao, Ya Zhao, Gang Li, Hua Xie, and Ling Jiang*

Cite This: J. Phys. Chem. A 2023, 127, 2819−2829

Read Online

ACCESS | Metrics & More | Article Recommendations | Supporting Information

ABSTRACT: Elucidating the autoxidation of volatile organic compounds (VOCs) is crucial to understanding the formation mechanism of secondary organic aerosols, but it has been proven to be challenging due to the complexity of reactions under atmospheric conditions. Here, we report a comprehensive theoretical study of atmospheric autoxidation in VOCs exemplified by the atmospherically important methacrolein (MACR), a major oxidation product of isoprene. The results indicate that the Cl-adducts and H-abstraction products of MACR readily react with O_2 and undergo subsequent isomerizations via H-shift and cyclization, forming a large variety of lowly and highly oxygenated organic molecules. In particular, the first- and third-generation oxidation products derived from the Cl-adducts and the methyl-H-abstraction complexes are dominated in the atmospheric autoxidation, for which the fractional yields are remarkably affected by the NO concentration. The present findings have important implications for a systematical understanding of the oxidation processes of isoprene-derived compounds in the atmospheric environments.

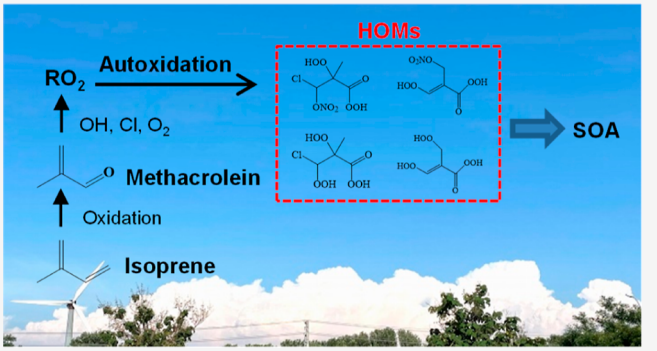

1. INTRODUCTION

Secondary organic aerosol (SOA), mainly formed from the atmospheric oxidation of volatile organic compounds (VOCs), constitutes a large majority of atmospheric particles and has a serious impact on the atmospheric climate, human health, and traffic safety.[1−3] Elucidating the stepwise formation mechanism of SOA in the complicated atmospheric environments is essential in understanding the initial steps of atmospheric aerosol formation and providing effective guidance for atmospheric haze control. Over the past few decades, extensive efforts were made to explore the SOA formation mechanisms from various VOCs, which provided great insights into the atmospheric chemistry.[4−7]

The autoxidation of VOCs plays an important role in the atmospheric chemistry,[8,9] degradation of olefinic liquid,[10] and combustion chemistry.[11] For instance, the autoxidation of organic compounds remarkably contributes to the generation and aging of atmospheric particulate matters.[12] The chemistry of atmospheric peroxy radical intermediates is also central to the autoxidation process, where the successive H-shift and O_2-addition reactions convert the VOC-derived peroxy radicals into highly oxygenated organic molecules (HOMs).[8,12−14] This direct autoxidation pathway begins with the conversion from the biogenic VOCs to very low-volatile organic vapors in large quantities.[15−17] The formation of hydroperoxy amides also evidences the potential atmospheric H-shift and autoxidation of amine-derived peroxy radicals.[18] These vapors exhibit significant mass yields in the gas phase and condense on aerosol surfaces.

Isoprene is the largest source of non-methane VOCs, with estimated emissions of 535 Tg $year^{-1}$.[19] Since isoprene possesses structural peculiarity with two double bonds, its oxidation by the radicals (i.e., OH, O_3, and NO_3) readily occurs in the atmosphere, making significant contributions to the sources of atmospheric organic particulate matters.[4,20−26] Such isoprene oxidations generate a large variety of products, which would affect the tropospheric oxidation capacity and associated chemical cycles of atmospheric trace gases.[27−29]

As one of the major products of isoprene oxidation,[4,30−32] methacrolein (MACR) and its oxidation are central to the formation of SOA. MACR was proposed to be highly reactive with Cl,[33−36] O_3,[37−39] OH,[40−45] and NO_3.[46,47] MACR oxidation was found to be a necessary step in the SOA formation from isoprene photooxidation,[4,25] in which the preservation of the four-carbon backbone in SOA would shed light into the gas-phase mechanism of the SOA precursor. Smog chamber experiments suggested that MACR could

Received: January 7, 2023
Revised: February 20, 2023
Published: March 20, 2023

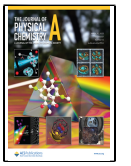

https://doi.org/10.1021/acs.jpca.3c00128
J. Phys. Chem. A 2023, 127, 2819−2829

undergo photooxidation to form methacrylic acid epoxide,[48] which is a major precursor for the isoprene-derived SOA tracer under high levels of nitrogen oxide (NO_x = NO + NO_2), with reminiscence of typical urban atmospheres.[48] 2-Methylglyceric acid evolved from MACR was found to undergo esterification to produce low-volatile oligoesters.[31,49] A successive cyclization-driven autoxidation mechanism was proposed in the reactions of allylic radicals generated from the H-abstraction of isoprene.[50] The Cl atoms are highly reactive and can profoundly affect the atmospheric compositions, especially in coastal urban areas.[51] However, systematic study on the Cl-initiated MACR reactions and subsequent autoxidation processes remains elusive thus far.

In this work, we investigated the autoxidation mechanisms and kinetics of the Cl-initiated MACR reactions and subsequent autoxidations under atmospheric conditions using a combined method of quantum chemical calculations and kinetics modeling. The results indicate that the Cl-addition and H-abstraction products of MACR readily react with O_2 and undergo isomerizations via H-shift and cyclization, forming a series of lowly oxygenated organic molecules and HOMs with potential contributions to the new particle formation. In particular, the first- and third-generation oxidation products derived from the Cl-adducts and the methyl-H-abstraction complexes are dominated in the MACR autoxidation, for which the fractional yields are remarkably affected by the NO concentrations.

2. METHODS

The structural information of the initial carbon center radicals was obtained from the previous study.[36] The most stable isomers of organic peroxy radicals (RO_2) produced from the oxidation of M_{Cl}, M_1, and M_2 were determined using the Molclus program.[52] The "gentor" tool in Molclus was used to generate an initial population of isomers via systematic structural scanning, namely, by regularly rotating the target dihedral angle of the target molecular isomer. The resulting initial isomer population was screened for the most stable RO_2 geometry by energetics calculations and used for the subsequent H-transfer, cyclization, and dissociation. The detailed screening process is described in Figure S1 in the Supporting Information.

Geometric optimization and frequency calculations of the reactants, transition states (TS), intermediates (IMs), and products involved in the subsequent autoxidation pathways were performed using the Gaussian 09 program package[53] at the M06-2X/6-311+G(d,p) level of theory.[54] The original structures of TSs were manually constructed based on the isomerization ways (H-shift, cyclization) of IMs in the autoxidation process and optimized using the Berny algorithm. Intrinsic reaction coordinate calculations were carried out for all transition states to confirm that the transition states connect the initial and final states. In the benchmark study, the single-point energy calculations of intermediates and transition states involved in the five isomerization processes of the peroxy radicals produced from the O_2-addition on M_2 were performed on top of the M06-2X/6-311+G(d,p) geometries at the ωB97XD/aug-cc-pVTZ, M06-2X/6-311+G(3df,2pd), M06-2X/aug-cc-pVTZ, CBS-QB3, and CCSD(T)/cc-pVTZ levels (see Table S1 for the details). Optimally, the ωB97XD/aug-cc-pVTZ method was selected for the single-point energy calculations.[55] The potential energy profiles were calculated at ωB97XD/aug-cc-pVTZ//M06-2X/6-311+G(d,p) level of theory, including the zero-point energy corrections.

The kinetics calculations of the unimolecular reactions were performed using the Master Equation Solver for Multi-energy Well Reactions (MESMER) program.[56] The reaction rate constants for each individual reaction step in the full system were calculated using the Rice−Ramsperger−Kassel−Marcus method. The harmonic frequencies and rotational constants were obtained from the M06-2X/6-311+G(d,p) calculation results, and the energy barriers were obtained from the results at the ωB97XD/aug-cc-pVTZ level of theory. The energy transfer was modeled using an exponential down model and the average energy transferred of ΔE_d = 200 cm^{-1} was used to simulate the collision energy between intermediates and bath gas molecule (N_2). The epsilon (K) and sigma (Å) parameters for a Lennard-Jones interaction potential for the intermediates were estimated by an empirical method proposed by Gilbert and Smith,[57] as listed in Table S2. The kinetics modeling was done at 298 K and 1 atm of pressure. The one-dimensional asymmetric Eckart-barrier approximation was employed to account for the tunneling correction of reactions in the main autoxidation process involving H-shift.[58] The yield was obtained by the ratio, where the numerator was the rate constant of each branch of the reaction path and the denominator was the sum of the rate constant of each branch of the reaction path in the same stage. The pseudo-first-order reaction rate constant (RO_2 with NO, HO_2, and O_2) and the reaction rate constant calculated by MESMER were used to calculate the yield, with the reference to the method in the literature.[50]

3. RESULTS AND DISCUSSION

The reaction of MACR with Cl yields initial adducts (labeled as M_{Cl}), in which the Cl atom is bound to the C(1) atom and the radical is located on the C(2) site (Scheme 1). The Cl atom can directly abstract the hydrogen atom from the aldehyde or the methyl group, forming the aldehyde-H-abstraction complex (M_1) and the methyl-H-abstraction complex (M_2) (Scheme 1), respectively. The mechanism for the abstraction from MACR has been recently discussed.[36] The reaction of M_x (x = Cl, 1, and 2) with the first, second, and third O_2 molecule produces the first-, second-, and third-generation oxidation intermediates, which are labeled as M_x-IM_a, M_x-IM_b, and M_x-IM_c, respectively. The following sections describe the successive autoxidation reactions of M_{Cl}, M_1, and M_2.

Scheme 1. Structures of M_{Cl}, M_1, and M_2[a]

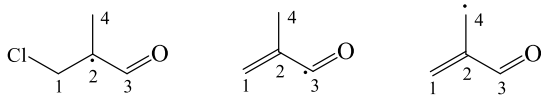

M_{Cl} M_1 M_2

[a]The positions of the C atoms are labeled for the convenience of discussion.

3.1. Potential Energy Profiles for Successive Autoxidation of M_{Cl}. The potential energy profiles of the M_{Cl} + O_2 reaction are shown in Figure 1. The addition of O_2 onto the C(2) site forms a peroxy radical (labeled M_{Cl}-IM_a), which is predicted to be exothermic (14.0 kcal mol^{-1}). M_{Cl}-IM_a undergoes isomerization to form three types of C-center

https://doi.org/10.1021/acs.jpca.3c00128
J. Phys. Chem. A 2023, 127, 2819−2829

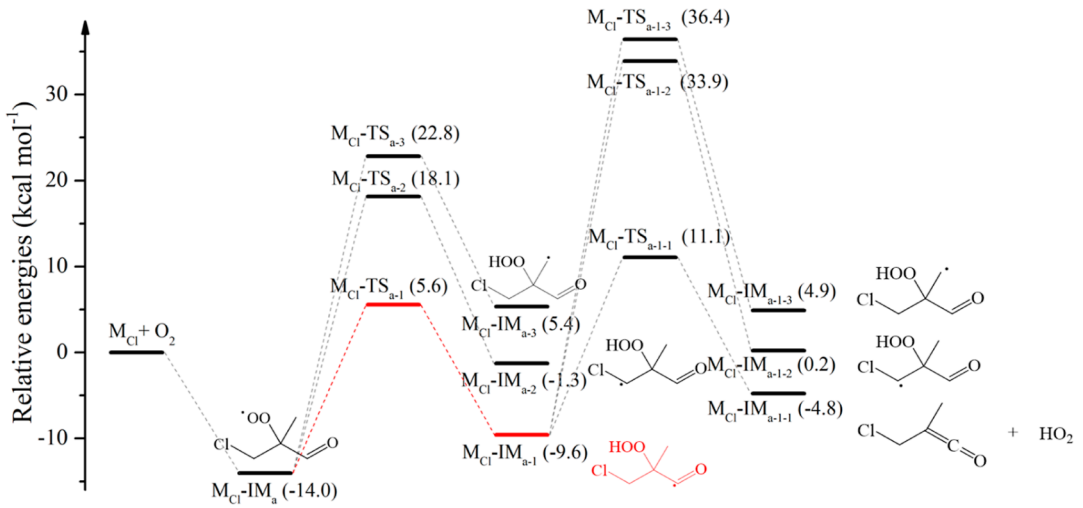

Figure 1. Potential energy profiles of the favorable isomerization pathways for M_{Cl}-IM_a formed from the reaction of M_{Cl} with O_2 calculated at the ωB97XD/aug-cc-pVTZ//M06-2X/6-311+G(d,p) level of theory. M_{Cl}-$IM_{a\text{-}n}$ is transformed from M_{Cl}-IM_a, and M_{Cl}-$IM_{a\text{-}n\text{-}m}$ is the product generated from the isomerization or dissociation channel of M_{Cl}-$IM_{a\text{-}n}$, where n = 1−3 and m = 1−3. The total energy of the reactants M_{Cl} + O_2 is set as zero (reference state).

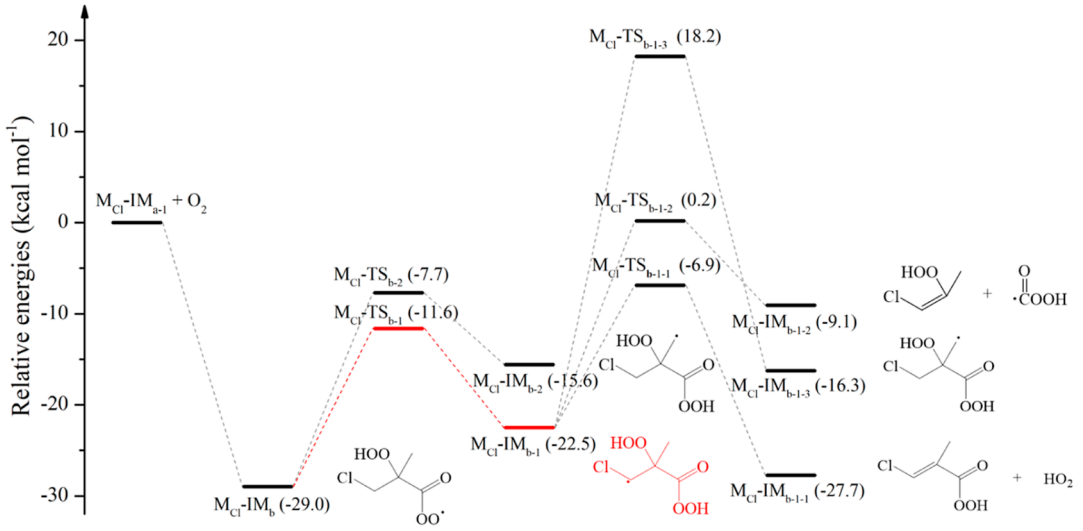

Figure 2. Potential energy profiles of the favorable isomerization pathways for M_{Cl}-IM_b formed from the reaction M_{Cl}-$IM_{a\text{-}1}$ with O_2 calculated at the ωB97XD/aug-cc-pVTZ//M06-2X/6-311+G(d,p) level of theory. The total energy of the reactants M_{Cl}-$IM_{a\text{-}1}$ + O_2 is set as zero (reference state).

radicals (M_{Cl}-$IM_{a\text{-}1}$, M_{Cl}-$IM_{a\text{-}2}$, and M_{Cl}-$IM_{a\text{-}3}$) via H-transfer from different groups. The barrier of transition state M_{Cl}-$TS_{a\text{-}1}$ (19.6 kcal mol^{-1}) is much lower than those of M_{Cl}-$TS_{a\text{-}2}$ (32.2 kcal mol^{-1}) and M_{Cl}-$TS_{a\text{-}3}$ (36.9 kcal mol^{-1}), suggesting that the formation of M_{Cl}-$IM_{a\text{-}1}$ via H-transfer from the aldehyde group is more favorable. Upon C−O bond cleavage, the dissociation of M_{Cl}-$IM_{a\text{-}1}$ produces M_{Cl}-$IM_{a\text{-}1\text{-}1}$ (C_4H_5OCl) and HO_2 with a barrier of 20.6 kcal mol^{-1}. The isomerization products of M_{Cl}-$IM_{a\text{-}1\text{-}2,3}$ and M_{Cl}-$IM_{a\text{-}1\text{-}2,3}$ are difficult to be formed via 1,3 H-shift because of high ring tension. The reaction rate constant of a typical C-centered radical with O_2 is ~3.2 × 10^7 s^{-1},[59] which is considerably faster than the predicted dissociation rate constant of the M_{Cl}-$IM_{a\text{-}1}$ → M_{Cl}-$IM_{a\text{-}1\text{-}1}$ + HO_2 reaction (1.7 × 10^{-2} s^{-1}). It thus appears that M_{Cl}-$IM_{a\text{-}1}$ might proceed to react with O_2 rather than its dissociation.

As shown in Figure 2, the M_{Cl}-$IM_{a\text{-}1}$ + O_2 → M_{Cl}-IM_b reaction is calculated to be exothermic by 29.0 kcal mol^{-1}, with the formation of a peroxy radical. M_{Cl}-IM_b transforms to C-centered radicals (M_{Cl}-$IM_{b\text{-}1}$ and M_{Cl}-$IM_{b\text{-}2}$) by 1,5 H-shift with energy barriers of 17.4 and 21.3 kcal mol^{-1}, respectively, forming C═O(OOH) groups. The endothermic energy of the M_{Cl}-IM_b → M_{Cl}-$IM_{b\text{-}1}$ reaction (6.5 kcal mol^{-1}) is smaller than that of the M_{Cl}-IM_b → M_{Cl}-$IM_{b\text{-}2}$ reaction (13.4 kcal mol^{-1}), indicating that the H-abstraction from the CH_2Cl unit is more favorable than that from the CH_3 group. Three possible pathways were explored for the subsequent unimolecular reaction of M_{Cl}-$IM_{b\text{-}1}$. Releasing HO_2 via C−O bond cleavage is predicted to be exothermic by 5.2 kcal mol^{-1} with a smallest barrier of 15.6 kcal mol^{-1}. The population of this dissociation product M_{Cl}-$IM_{b\text{-}1\text{-}1}$ could be small because the C-center radical M_{Cl}-$IM_{b\text{-}1}$ might prefer to react with O_2 in the atmosphere because of its fast reaction rate.[59] The potential energy profiles of the subsequent reaction for M_{Cl}-$IM_{b\text{-}1}$ with O_2 are shown in Figure 3. The M_{Cl}-$IM_{c\text{-}1}$ peroxy radical is generated by 1,5 H-shift, which is predicted to be endothermic

https://doi.org/10.1021/acs.jpca.3c00128
J. Phys. Chem. A 2023, 127, 2819−2829

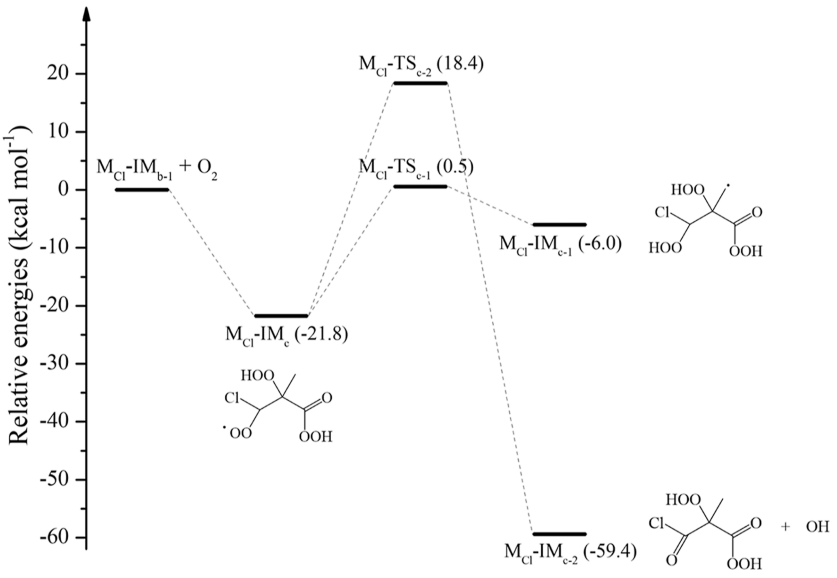

Figure 3. Potential energy profiles of the favorable isomerization pathways for M_{Cl}-IM_c formed from the reaction M_{Cl}-IM_{b-1} with O_2 at the ωB97XD/aug-cc-pVTZ//M06-2X/6-311+G(d,p) level. The total energy of the reactants M_2-IM_{b-1} + O_2 is set as zero (reference state).

by 15.8 kcal mol^{-1} with a barrier of 22.3 kcal mol^{-1}. In contrast to the unimolecular isomerization of a given RO_2, its bimolecular reaction with NO/HO_2 is generally considered to be the main competitive pathway. Therefore, the autoxidation of M_{Cl} might be mainly terminated by the reaction of M_{Cl}-IM_{c-1} with NO/HO_2.

3.2. Potential Energy Profiles for Successive Autoxidation of M_1 and M_2. The potential energy profiles for the reaction of M_1 with O_2 are shown in Figure S2. The reaction of M_1 with O_2 to form M_1-IM_a is calculated to be highly exothermic by 29.8 kcal mol^{-1}, which is more thermodynamically favorable than that of M_{Cl} with O_2 (14.0 kcal mol^{-1}). This could be rationalized by the fact that M_1 possesses an aldehyde radical, whereas M_{Cl} does not. The subsequent isomerization of M_1-IM_a might proceed by either cyclization via the attack of the terminal O atom by the unsaturated C atoms [C(1) and C(2)] or H-shift via the attack of the terminal O atom of M_1-IM_a by the high-activity H atoms of CH_2 and CH_3. M_1-IM_{a-1} is formed by cyclization with a smallest barrier of 16.7 kcal mol^{-1}, resulting in a four-membered ring. The following allylic radical M_1-IM_{a-2} is generated by 1,5 H-shift, which is exothermic by 15.8 kcal mol^{-1} with a barrier of 18.0 kcal mol^{-1}. The formation of M_1-IM_{a-3} and M_1-IM_{a-4} needs to overcome a higher barrier of 20.8 and 24.2 kcal mol^{-1}, respectively. With the courtesy of relatively low isomerization barrier, M_1-IM_{a-1} was selected as the candidate for the subsequent oxidations. The reaction of M_1-IM_{a-1} with O_2 is predicted to be exothermic by 26.1 kcal mol^{-1} with a negligible barrier (Figure S2b), which is more favorable than its dissociation with a barrier of 21.0 kcal mol^{-1} (Figure S2a). The subsequent H-abstraction of M_1-IM_b (1,5 H-shift) needs to overcome a large barrier of 26.3 kcal mol^{-1}, suggesting a lower activity of H atom in the CH_3 group of M_1-IM_{b-1}. Consequently, M_1-IM_{b-1} would be the terminal intermediate of the autoxidation of M_1, and its bimolecular reaction with NO/HO_2 will be discussed later (vide infra).

The potential energy profiles for the reaction of M_2 with O_2 and the subsequent isomerization are shown in Figure S3. The M_2 + O_2 → M_2-IM_a reaction is calculated to be exothermic by 15.9 kcal mol^{-1}. Due to the presence of the unsaturated C atom, M_2-IM_a might be isomerized to M_2-IM_{a-n} (n = 1−5) via H-abstraction and/or cyclization. Based on the high activity of the H atom in the CHO group, the formation of M_2-IM_{a-1} via the 1,5 H-shift is the most favorable pathway with an energy barrier by 17.8 kcal mol^{-1}. Analogous to M_{Cl}-IM_{a-1} and M_1, the dissociation and isomerization of M_2-IM_{a-1} are difficult to compete with its rapid reaction with O_2. As shown in Figure S4, the addition of O_2 onto the C═O group of M_2-IM_{a-1} is calculated to be exothermic by 32.3 kcal mol^{-1}. Subsequent transformations of M_2-IM_b have four possible pathways to form M_2-IM_{b-n} (n = 1−4) by H-abstraction and/or cyclization. Among these isomerization processes, the unsaturated M_2-IM_{b-1} is formed by H-abstraction from the CH_2 group, which is exothermic by 3.7 kcal mol^{-1} with a smallest barrier of 16.3 kcal mol^{-1}. M_2-IM_{b-2} is generated by cyclization (with a four-membered ring), which is endothermic by 4.6 kcal mol^{-1} with a barrier of 17.6 kcal mol^{-1}. Based on the criterion of energy barrier, M_2-IM_{b-1} was selected as the first candidate to study the next step of oxidation. As shown in Figure S4, both the dissociation and isomerization of M_2-IM_{b-1} are all kinetically difficult. Following the preferential reaction of the C-centered radical with O_2, the M_2-IM_{b-1} + O_2 → M_2-IM_{c1} reaction is predicted to be exothermic by 19.9 kcal mol^{-1} (Figure S5). The subsequent isomerization of M_2-IM_{c1} is predicted to be unfavorable because of the presence of the high energy barrier. Since the barrier height of M_2-TS_{b-2} is close to that of M_2-TS_{b-1} (Figure S4), M_2-IM_{b-2} was then considered as the second candidate to explore the subsequent reactions.

As illustrated in Figure S6, the reaction of M_2-IM_{b-2} with O_2 is calculated to be exothermic by 25.1 kcal mol^{-1}, forming M_2-IM_{c2}. Due to the high ring tension for the 1,3 H-shift between the terminal O atom of the peroxy radical and the connected CH_2 group in M_2-IM_{c2}, there is only one feasible pathway for the H-shift. Accordingly, M_2-IM_{c2} undergoes 1,5 H-shift isomerization to produce M_2-IM_{c2-1}, which is slightly endothermic with a barrier of 19.5 kcal mol^{-1}. Due to the instability of M_2-IM_{c2-1}, there are two facile dissociation pathways. First, since the OOH group is connected with the alkyl radical, the O−O bond can be readily fractured, and M_2-IM_{c2-1} dissociates into M_2-IM_{c2-1-1} and OH via a barrier-free

https://doi.org/10.1021/acs.jpca.3c00128
J. Phys. Chem. A 2023, 127, 2819−2829

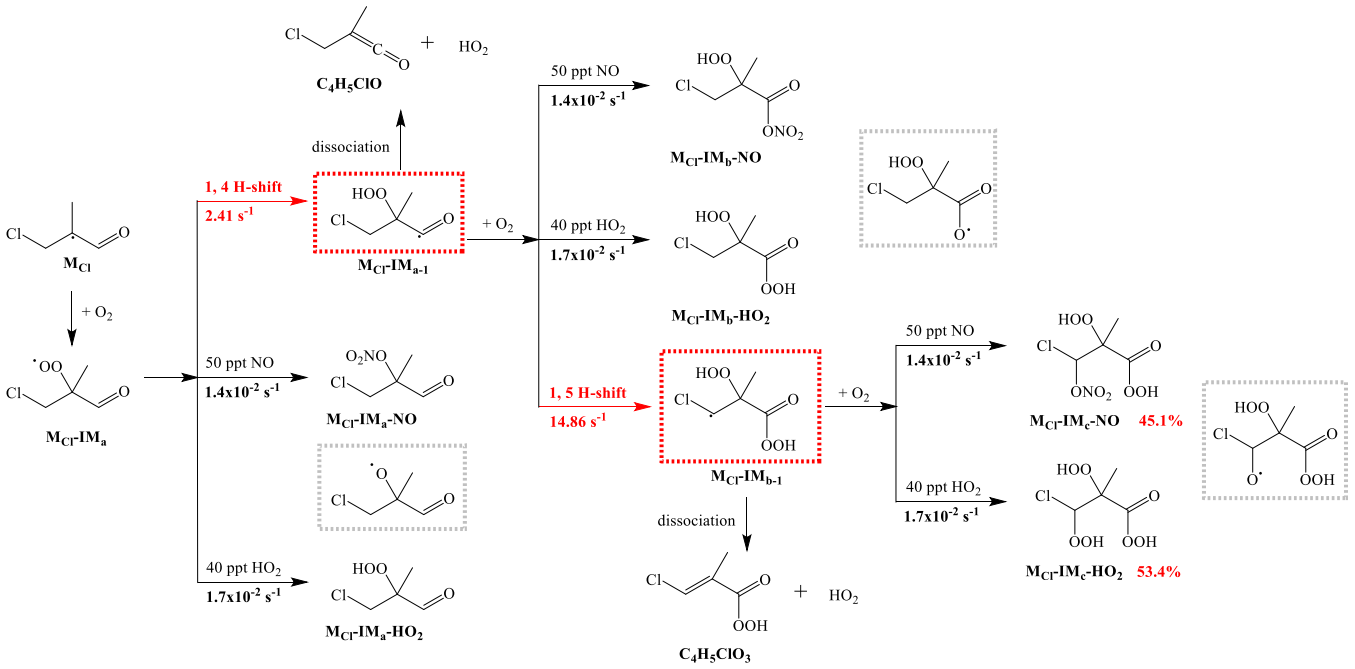

Figure 4. Main pathways for the atmospheric reactions of alkyl radical M_{Cl}. The red dashed box represents the most favorable intermediate in the aforementioned isomerization processes. The alkoxy radicals within the gray dashed box refer to the products in the bimolecular reactions of RO_2 + NO and RO_2 + HO_2. The most favorable autoxidation process is indicated by the red arrow. The reaction rate constant (s^{-1}) is indicated below the arrow. The products with fractional yields (%) less than 1% are not indicated.

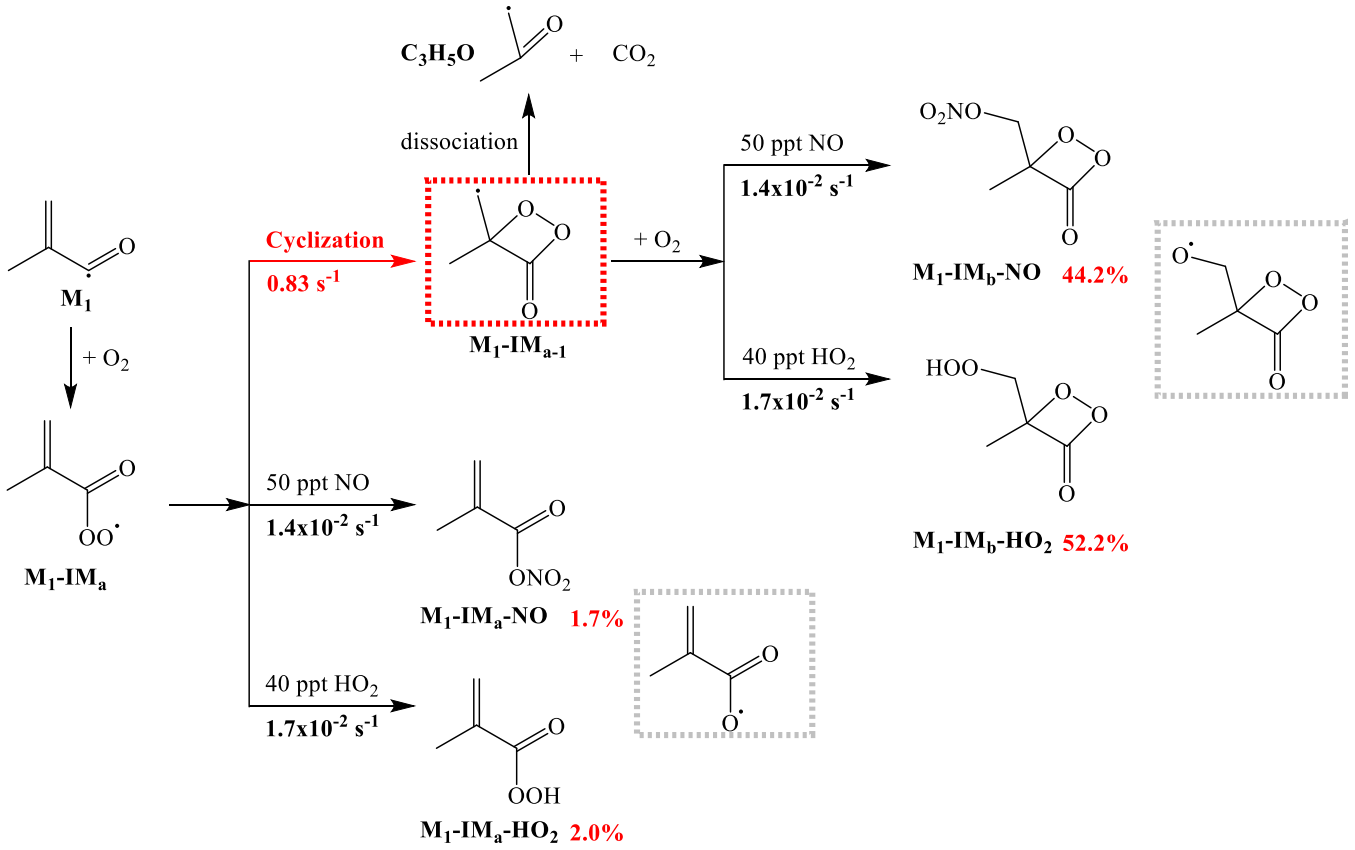

Figure 5. Main pathways for the atmospheric oxidations of M_1. The red dashed box represents the most favorable intermediate in the aforementioned isomerization processes. The alkoxy radicals within the gray dashed box refer to the products in the bimolecular reactions of RO_2 + NO and RO_2 + HO_2. The most favorable autoxidation process is indicated by the red arrow. The reaction rate constant (s^{-1}) is indicated below the arrow. The products with fractional yields (%) less than 1% are not indicated.

https://doi.org/10.1021/acs.jpca.3c00128
J. Phys. Chem. A 2023, 127, 2819−2829

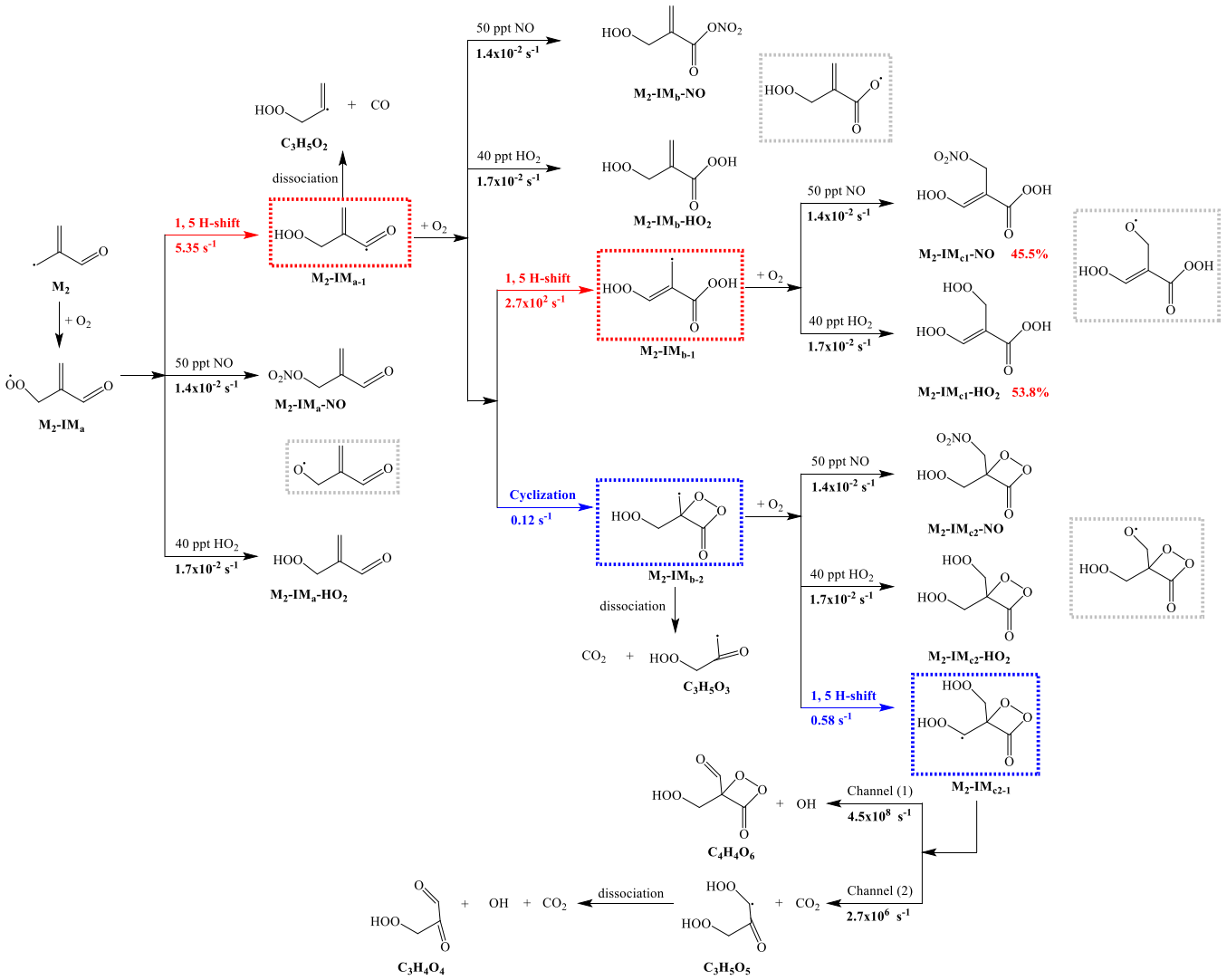

Figure 6. Main pathways for the atmospheric reactions of alkyl radical M_2. The red dashed box represents the most favorable intermediate in the aforementioned isomerization processes. The blue dashed box represents the second favorable intermediate. The alkoxy radicals within the gray dashed box refer to the products in the bimolecular reactions of RO_2 + NO and RO_2 + HO_2. The most favorable autoxidation process is indicated by the red arrow. The reaction rate constant (s^{-1}) is indicated below the arrow. The products with fractional yields (%) less than 1% are not indicated.

transition state. On the other hand, the M_2-IM_{c-1} → M_2-IM_{c-1-2} + CO_2 reaction is highly exothermic by 99.2 kcal mol^{-1} with a small barrier of 7.9 kcal mol^{-1}. M_2-IM_{c-1-2} releases OH to produce M_2-$IM_{c-1-2-1}$, which is predicted to be both thermodynamically exothermic and kinetically facile with a small barrier of 8.6 kcal mol^{-1}.

The aforementioned results address the favorable autoxidation pathways for M_{Cl}, M_1, and M_2. The best candidates of RO_2 radical chain reactions for each oxidation step were selected to analyze the thermodynamics and kinetics. The atmospheric reactions of RO_2 with NO and HO_2 will be discussed in the next section.

3.3. Kinetics of Main Reaction Pathways for M_{Cl}, M_1, and M_2 in Different Conditions. In general, the radical chain reaction is terminated by the bimolecular reaction of RO_2 with NO and HO_2 under atmospheric conditions. The reaction of RO_2 with NO is proposed to form both alkoxy radicals plus NO_2 and organic nitrates. The reaction of RO_2 with HO_2 generates hydroperoxides.[60−62] The concentration of NO and HO_2 ([NO] and [HO_2]) would be the key factor in affecting the reaction rates. Under clean atmospheric conditions (i.e., forest), the average concentration of NO and HO_2 is ∼50 ppt.[63,64] Under polluted conditions, the average concentration of NO increases to ∼5 ppb, whereas that of HO_2 is virtually unchanged (∼50 ppt).[63,64] The typical reaction rate constant of RO_2 with NO and HO_2 is k_{RO_2+NO} = 9.0×10^{-12} cm^3 $molecule^{-1}$ s^{-1} and $k_{RO_2+HO_2}$ = 1.7×10^{-11} cm^3 $molecule^{-1}$ s^{-1},[65,66] respectively. The pseudo-first-order rate of RO_2 with NO and HO_2 under clean atmospheric conditions was determined to be 1.4×10^{-2} and 1.7×10^{-2} s^{-1}, respectively.[27,63,64] In this work, the products generated from the reactions of M_x-IM_y (x = Cl, 1, 2; y = a, b, c) with NO and HO_2 are marked as M_x-IM_y-NO and M_x-IM_y-HO_2. For the kinetic issues of most favorable reaction pathways, the unimolecular reaction rate constants were calculated using the MESMER program. The dependence of [NO] was studied for the products with yields larger than 1%.

The main atmospheric oxidation pathways of M_{Cl} are proposed in Figure 4. It can be inferred from the analysis in

https://doi.org/10.1021/acs.jpca.3c00128
J. Phys. Chem. A 2023, 127, 2819−2829

Section 3.1 that the most favorable autoxidation pathway of M_{Cl} is $M_{Cl} \rightarrow M_{Cl}\text{-}IM_a \rightarrow M_{Cl}\text{-}IM_{a\text{-}1} \rightarrow M_{Cl}\text{-}IM_{b\text{-}1}$. The reaction of the first-generation oxidation intermediate $M_{Cl}\text{-}IM_a$ with NO and HO_2 produces $M_{Cl}\text{-}IM_a\text{-}NO$ ($C_4H_6NClO_4$, organonitrate) and $M_{Cl}\text{-}IM_a\text{-}HO_2$ ($C_4H_7ClO_3$, 3-chloro-2-hydroperoxy-2-methylpropanal) with low fractional yields. The reaction of the second-generation oxidation intermediate $M_{Cl}\text{-}IM_b$ with NO and HO_2 forms $M_{Cl}\text{-}IM_b\text{-}NO$ ($C_4H_6ClNO_6$, organic nitric anhydride) and $M_{Cl}\text{-}IM_b\text{-}HO_2$ ($C_4H_7ClO_5$, peroxycarboxylic acid), also with relatively low fractional yields. $M_{Cl}\text{-}IM_b\text{-}NO$ consists of six O atoms and one OOH group promoting the H-shift isomerization for RO_2, featuring the characteristics of HOMs. The reaction of the third-generation oxidation intermediate $M_{Cl}\text{-}IM_c$ with NO and HO_2 generates $M_{Cl}\text{-}IM_c\text{-}NO$ ($C_4H_6ClNO_8$, organonitrate) and $M_{Cl}\text{-}IM_c\text{-}HO_2$ ($C_4H_7ClO_7$, peroxycarboxylic acid) with high fractional yields of 45.1 and 53.4%, respectively. There are two OOH groups in $M_{Cl}\text{-}IM_c\text{-}NO$ and $M_{Cl}\text{-}IM_c\text{-}HO_2$ and the number of O atoms is more than seven, confirming their identity as HOMs.

Figure 5 shows the possible atmospheric oxidation pathways of M_1. The reaction of the first-generation oxidation intermediate $M_1\text{-}IM_a$ with NO and HO_2 forms $M_1\text{-}IM_a\text{-}NO$ and $M_1\text{-}IM_a\text{-}HO_2$ with small fractional yields of 1.7 and 2.0%, respectively. It is worth mentioning that $M_1\text{-}IM_a\text{-}HO_2$ ($C_4H_6O_3$) possesses the same molecular weight as $C_5H_{10}O_2$ (m/z = 102) that was observed in the previous experiments.[67,68] Therefore, $M_1\text{-}IM_a\text{-}HO_2$ might contribute to the m/z = 102 species in the isoprene oxidation reaction. As the reaction rate for the isomerization of $M_1\text{-}IM_a$ ($\sim$0.83 s^{-1}) is slightly larger than that its reaction with NO (1.4×10^{-2} s^{-1}) and HO_2 (1.7×10^{-2} s^{-1}), the fractional yield of the products $M_1\text{-}IM_b\text{-}NO$ ($C_4H_5NO_6$, organonitrate) and $M_1\text{-}IM_b\text{-}HO_2$ ($C_4H_6O_5$, hydroperoxide) reaches up to 44.2 and 52.2%, respectively. These final products do not belong to the HOMs due to the lack of sufficient oxygen atoms. Consequently, it would be hard for M_1 to undergo multiple autoxidation steps to generate HOMs.

The main atmospheric oxidation pathways of M_2 are suggested in Figure 6. The most favorably successive autoxidation pathway is M_2 (C_4H_5O) $\rightarrow$ $M_2\text{-}IM_{a\text{-}1}$ ($C_4H_5O_3$) $\rightarrow$ $M_2\text{-}IM_{b\text{-}2}$ ($C_4H_5O_5$) $\rightarrow$ $M_2\text{-}IM_{c2\text{-}1}$ ($C_4H_5O_7$). The radical chain reaction of M_2 is terminated by the rapid dissociation of $M_2\text{-}IM_{c2\text{-}1}$. Under 50 ppt NO and 40 ppt HO_2 conditions, the reaction of the first-generation oxidation intermediate $M_2\text{-}IM_a$ with NO and HO_2 forms $M_2\text{-}IM_a\text{-}NO$ and $M_2\text{-}IM_a\text{-}HO_2$ with low fractional yields. The fractional yields of the second-generation oxidation products ($M_2\text{-}IM_b\text{-}NO$ and $M_2\text{-}IM_b\text{-}HO_2$) are also less than 1%. With the addition of O_2 to $M_2\text{-}IM_{a\text{-}1}$, there are two branches driven by H-shift and cyclization with the formation of $M_2\text{-}IM_{b\text{-}1}$ and $M_2\text{-}IM_{b\text{-}2}$, by which the addition of the third O_2 molecule proceeds. The radical chain reaction of $M_2\text{-}IM_{b\text{-}1}$ with O_2 produces unsaturated $M_2\text{-}IM_{c1}\text{-}NO$ ($C_4H_5NO_8$, organonitrate) and $M_2\text{-}IM_{c1}\text{-}HO_2$ ($C_4H_6O_7$, peroxycarboxylic acid), which exhibit the characteristics of HOMs and a large fractional yield, suggesting a dominant role in the autoxidation of M_2. The intermediate $M_2\text{-}IM_{c2\text{-}1}$ generated from the unimolecular reaction of $M_2\text{-}IM_{b\text{-}2}$ undergoes successive dissociation reactions and finally generates a series of fragments. For the dissociation of $M_2\text{-}IM_{c2\text{-}1}$, the reaction rate constant in channel (1) (4.5×10^8 s^{-1}) is much large than that in channel (2) (2.7×10^6 s^{-1}), implying that $C_3H_4O_4$ (3-hydroperoxy-2-oxopropanal) generated from the latter is not a dominated product. These results suggest that the assignment of $C_3H_4O_4$ (malonic acid) in the previous studies of isoprene oxidation might be reconsidered.[50]

In the whole autoxidation process, the oxidation of alkoxy radicals is also a competitive reaction pathway. For the alkoxy radicals of the bimolecular reactions of M_{Cl} and M_2-derived peroxy radical with NO/HO_2 in the first- and second-generation oxidations, the yield is relatively low, whereas that of alkoxy radicals generated from the third-generation oxidation accounts for a large proportion. With the structure–activity relationships[69,70] and the lower number of oxygen atoms of alkoxy radicals in the first- and second-generation oxidations, the possibility of the alkoxy radical to produce HOM through multistep autoxidation is lower. Only those alkoxy radicals with higher number of oxygen atoms have the potential for the production of HOMs. The alkoxy radicals generated from the oxidation of M_1 possess a similar situation. Thus, further oxidation reaction of alkoxy radicals will not be discussed explicitly in the whole autoxidation process. With the conditions varying from clean to polluted atmospheric environments, the change of [NO] is much larger than that of [HO_2].[63,64] The above results indicate the M_{Cl}- and M_2-derived products exhibit the potential formation of HOMs instead of the M_1-derived products. Accordingly, the dependence of [NO] on the fractional yields of the main products for M_{Cl} and M_2 was studied, and the results are shown in Figure 7.

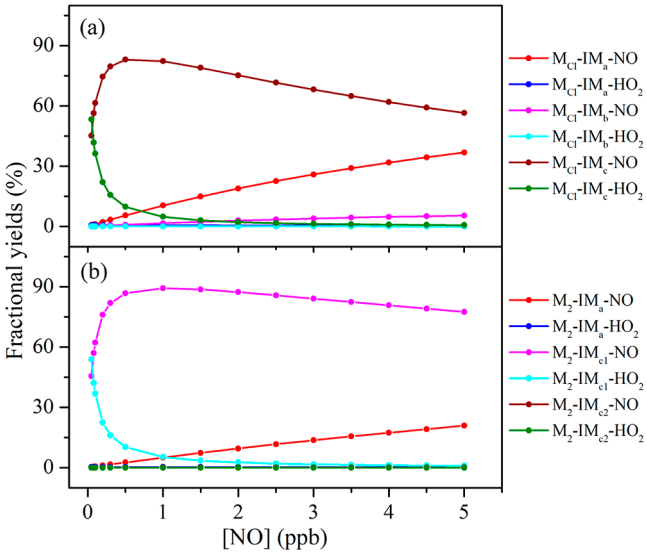

Figure 7. Simulated fractional yields of the main products from the autoxidation pathways of M_{Cl} and M_2 as a function of [NO] (ppb).

For M_{Cl} (Figure 7a), a remarkable effect of [NO] on the fractional yield is observed for the first-generation oxidation products, $M_{Cl}\text{-}IM_a\text{-}NO$ and $M_{Cl}\text{-}IM_a\text{-}HO_2$. For instance, as [NO] increases from 0.05 to 5 ppb (from clean to polluted atmosphere), the yield of $M_{Cl}\text{-}IM_a\text{-}NO$ increases from 0.6 to 36.8%, whereas that of $M_{Cl}\text{-}IM_a\text{-}HO_2$ decreases from 0.7 to 0.4%. For the highly oxygenated products, the yields of $M_{Cl}\text{-}IM_c\text{-}NO$ and $M_{Cl}\text{-}IM_c\text{-}HO_2$ increase obviously when [NO] increases from 0.05 to 0.5 ppb, and then it drops down. This indicates that the high [NO] is the main obstacle that affects the autoxidation of M_{Cl} to form HOMs, which might be attributed to the suppression of the H-shift isomerization by

https://doi.org/10.1021/acs.jpca.3c00128
J. Phys. Chem. A 2023, 127, 2819–2829

the rapid reaction of RO_2 and NO. A similar effect of [NO] on the fractional yields of main products is also obtained for the autoxidation of M_2, as shown in Figure 7b. With the increase of [NO] from 0.05 to 5 ppb, the yield of M_2-IM_a-NO increases from 0.3 to 20.9%, whereas that of M_2-IM_a-HO_2 decreases from 0.3 to 0.2%. It is worth noting that the yield of M_2-IM_{c1}-NO increases from 45.5 to 89.3% with the increase of [NO] to 1 ppb. It implies that the slight increase of [NO] under forest atmospheric conditions promotes the generation of highly oxygenated products M_2-$IM_{c1,2}$-NO ($C_4H_5NO_8$). The yields of M_2-IM_{c1}-HO_2 ($C_4H_6O_7$) decrease gradually due to the rapid growth of M_2-IM_a-NO. Overall, the first- and third-generation oxidation intermediates M_{Cl}-IM_a-NO ($C_4H_6NClO_4$), M_2-IM_a-NO ($C_4H_5NO_4$), M_{Cl}-IM_c-NO ($C_4H_6NClO_8$), and M_2-IM_{c1}-NO ($C_4H_5NO_8$) are the dominant products under high NO concentrations.

4. ATMOSPHERIC IMPLICATION AND CONCLUSIONS

This work addresses the possible autoxidation pathways for the Cl-addition and H-abstraction products of MACR, where both H-shift and cyclization occur during the isomerization of RO_2 generated from M_{Cl}, M_1, and M_2. The final products mainly include organonitrates, aldehydes, hydroperoxides, peroxycarboxylic acids, and organic nitric anhydrides. This study also proposes the ability of this C_4 aldehyde to generate HOMs, providing a plausible reference for assessing the possible structures of C_4 highly oxidized products. M_{Cl} and M_2 undergo consecutive H-shifts to generate highly oxidized products. The cyclization-driven isomerization of M_2 only contributes to a small part of highly oxidized products. At 297 K and 760 Torr, the branching ratio of M_{Cl}, M_1, and M_2 is about 86, 12, and 2%, respectively.[36] Based on a higher fractional yield of M_{Cl} than those of M_1 and M_2, the terminal autoxidation products would be dominated by M_{Cl}-derived complexes. As pointed out previously,[71] the Cl-addition products are also dominant in the reaction of isoprene and Cl; one of two addition products could not undergo multistep oxidation to generate HOMs, and the main products are MACR, methyl vinyl ketone, and 1-chloro-3-methyl-3-buten-2-one, which simultaneously increase the initial concentration of MACR involved in the reaction. Another addition product undergoes O_2-addition reactions twice and finally generates $C_5H_8NClO_5$, but its degree of oxidation is not high enough based on the definition of HOMs.[71] For the H-abstraction product of isoprene, the O/C value of HOMs driven by cyclization is 1.4.[50] However, the values of O/C for terminal autoxidation products derived from M_{Cl} and M_2 reach up to 2, suggesting that these highly oxidized products with more oxygen atoms might make a larger contribution to the early growth of nanoparticles than the C_5 highly oxidized products stemmed from isoprene.

The HOMs proposed in this work would contribute to the condensational growth at all sizes, ranging from the newly formed particles (nanocondensation nuclei, ~1 nm) to cloud condensation nuclei (~100 nm).[15] The yield of highly oxidized products studied here is considerably affected by [NO]. Under low [NO] conditions, the M_{Cl}- and M_2-derived complexes could generate highly oxidized products, which might have an impact on the early growth of nanoparticles in coastal forest areas. Under high [NO] conditions, the lowly oxidized products are readily formed instead of the highly oxidized products, which is consistent with the previous results that NO with high concentration consumes more RO_2.[23] These findings provide crucial information for a systematical understanding of the autoxidative potentials of MACR and expand a large variety of final products from isoprene. It is hoped that the present results will stimulate further study of various oxidation reactions of VOC-derived compounds in the atmospheric environments.

■ ASSOCIATED CONTENT

Supporting Information

The Supporting Information is available free of charge at https://pubs.acs.org/doi/10.1021/acs.jpca.3c00128.

Flow chart of multiconformers search; potential energy profiles of reactions in the M1 and M2 autoxidation pathways; detailed data in the benchmark study of single-point energy calculations; Lennard-Jones parameters of intermediates; calculated rate constant values of the main reaction pathways for M_{Cl}, M_1, and M_2; and cartesian coordinates of intermediates and transition states for the reactions of M_{Cl}, M_1, and M_2 (PDF)

■ AUTHOR INFORMATION

Corresponding Author

Ling Jiang − *State Key Laboratory of Molecular Reaction Dynamics, Dalian Institute of Chemical Physics, Chinese Academy of Sciences, Dalian 116023, China; Hefei National Laboratory, Hefei 230088, China;* orcid.org/0000-0002-8485-8893; Email: ljiang@dicp.ac.cn

Authors

Zhaoyan Zhang − *State Key Laboratory of Molecular Reaction Dynamics, Dalian Institute of Chemical Physics, Chinese Academy of Sciences, Dalian 116023, China; University of Chinese Academy of Sciences, Beijing 100049, China*

Chong Wang − *State Key Laboratory of Molecular Reaction Dynamics, Dalian Institute of Chemical Physics, Chinese Academy of Sciences, Dalian 116023, China; University of Chinese Academy of Sciences, Beijing 100049, China*

Yingqi Zhao − *State Key Laboratory of Molecular Reaction Dynamics, Dalian Institute of Chemical Physics, Chinese Academy of Sciences, Dalian 116023, China; University of Chinese Academy of Sciences, Beijing 100049, China*

Ya Zhao − *State Key Laboratory of Molecular Reaction Dynamics, Dalian Institute of Chemical Physics, Chinese Academy of Sciences, Dalian 116023, China*

Gang Li − *State Key Laboratory of Molecular Reaction Dynamics, Dalian Institute of Chemical Physics, Chinese Academy of Sciences, Dalian 116023, China;* orcid.org/0000-0001-5984-111X

Hua Xie − *State Key Laboratory of Molecular Reaction Dynamics, Dalian Institute of Chemical Physics, Chinese Academy of Sciences, Dalian 116023, China;* orcid.org/0000-0003-2091-6457

Complete contact information is available at: https://pubs.acs.org/10.1021/acs.jpca.3c00128

Notes

The authors declare no competing financial interest.

■ ACKNOWLEDGMENTS

The authors gratefully acknowledge the Dalian Coherent Light Source (DCLS) for support and assistance. This work was supported by the National Natural Science Foundation of

China (nos. 22125303, 92061203, 22103082, 22273101, and 22288201), the National Key Research and Development Program of China (no. 2021YFA1400501), the Innovation Program for Quantum Science and Technology (no. 2021ZD0303304), the Dalian Institute of Chemical Physics (no. DICP DCLS201702), and the Chinese Academy of Sciences (no. GJJSTD20220001).

REFERENCES

(1) Brauer, M.; Freedman, G.; Frostad, J.; van Donkelaar, A.; Martin, R. V.; Dentener, F.; Dingenen, R.; Estep, K.; Amini, H.; Apte, J. S.; et al. Ambient Air Pollution Exposure Estimation for the Global Burden of Disease 2013. *Environ. Sci. Technol.* **2016**, *50*, 79−88.

(2) Shiraiwa, M.; Ueda, K.; Pozzer, A.; Lammel, G.; Kampf, C. J.; Fushimi, A.; Enami, S.; Arangio, A. M.; Fröhlich-Nowoisky, J.; Fujitani, Y.; et al. Aerosol Health Effects from Molecular to Global Scales. *Environ. Sci. Technol.* **2017**, *51*, 13545−13567.

(3) Lewis, A. C. The Changing Face of Urban Air Pollution. *Science* **2018**, *359*, 744−745.

(4) Wennberg, P. O.; Bates, K. H.; Crounse, J. D.; Dodson, L. G.; McVay, R. C.; Mertens, L. A.; Nguyen, T. B.; Praske, E.; Schwantes, R. H.; Smarte, M. D.; et al. Gas-Phase Reactions of Isoprene and Its Major Oxidation Products. *Chem. Rev.* **2018**, *118*, 3337−3390.

(5) Kirkby, J.; Curtius, J.; Almeida, J.; Dunne, E.; Duplissy, J.; Ehrhart, S.; Franchin, A.; Gagné, S.; Ickes, L.; Kürten, A.; et al. Role of Sulphuric Acid, Ammonia and Galactic Cosmic Rays in Atmospheric Aerosol Nucleation. *Nature* **2011**, *476*, 429−433.

(6) Yao, L.; Garmash, O.; Bianchi, F.; Zheng, J.; Yan, C.; Kontkanen, J.; Junninen, H.; Mazon, S. B.; Ehn, M.; Paasonen, P.; et al. Atmospheric New Particle Formation from Sulfuric Acid and Amines in a Chinese Megacity. *Science* **2018**, *361*, 278−281.

(7) Rastak, N.; Pajunoja, A.; Acosta Navarro, J. C. A.; Ma, J.; Song, M.; Partridge, D. G.; Kirkevåg, A.; Leong, Y.; Hu, W. W.; Taylor, N. F.; et al. Microphysical Explanation of the RH-Dependent Water Affinity of Biogenic Organic Aerosol and Its Importance for Climate. *Geophys. Res. Lett.* **2017**, *44*, 5167−5177.

(8) Lim, Y. B.; Ziemann, P. J. Products and Mechanism of Secondary Organic Aerosol Formation from Reactions of n-Alkanes with OH Radicals in the Presence of NO_X. *Environ. Sci. Technol.* **2005**, *39*, 9229−9236.

(9) Claeys, M.; Graham, B.; Vas, G.; Wang, W.; Vermeylen, R.; Pashynska, V.; Cafmeyer, J.; Guyon, P.; Andreae, M. O.; Artaxo, P.; et al. Formation of Secondary Organic Aerosols through Photooxidation of Isoprene. *Science* **2004**, *303*, 1173−1176.

(10) Porter, N. A. Mechanisms for the Autoxidation of Polyunsaturated Lipids. *Acc. Chem. Res.* **1986**, *19*, 262−268.

(11) Cox, R. A.; Cole, J. A. Chemical Aspects of the Autoignition of Hydrocarbon-Air Mixtures. *Combust. Flame* **1985**, *60*, 109−123.

(12) Crounse, J. D.; Nielsen, L. B.; Jørgensen, S.; Kjaergaard, H. G.; Wennberg, P. O. Autoxidation of Organic Compounds in the Atmosphere. *J. Phys. Chem. Lett.* **2013**, *4*, 3513−3520.

(13) Wang, Z.; Popolan-Vaida, D. M.; Chen, B.; Moshammer, K.; Mohamed, S. Y.; Wang, H.; Sioud, S.; Raji, M. A.; Kohse-Höinghaus, K.; Hansen, N.; et al. Unraveling the Structure and Chemical Mechanisms of Highly Oxygenated Intermediates in Oxidation of Organic Compounds. *Proc. Natl. Acad. Sci. U.S.A.* **2017**, *114*, 13102−13107.

(14) Bianchi, F.; Kurtén, T.; Riva, M.; Mohr, C.; Rissanen, M. P.; Roldin, P.; Berndt, T.; Crounse, J. D.; Wennberg, P. O.; Mentel, T. F.; et al. Highly Oxygenated Organic Molecules (HOM) from Gas-Phase Autoxidation Involving Peroxy Radicals: A Key Contributor to Atmospheric Aerosol. *Chem. Rev.* **2019**, *119*, 3472−3509.

(15) Ehn, M.; Thornton, J. A.; Kleist, E.; Sipilä, M.; Junninen, H.; Pullinen, I.; Springer, M.; Rubach, F.; Tillmann, R.; Lee, B.; et al. A Large Source of Low-Volatility Secondary Organic Aerosol. *Nature* **2014**, *506*, 476−479.

(16) Ehn, M.; Kleist, E.; Junninen, H.; Petäjä, T.; Lönn, G.; Schobesberger, S.; Dal Maso, M.; Trimborn, A.; Kulmala, M.; Worsnop, D. R.; et al. Gas Phase Formation of Extremely Oxidized Pinene Reaction Products in Chamber and Ambient Air. *Atmos. Chem. Phys.* **2012**, *12*, 5113−5127.

(17) Zhao, J.; Ortega, J.; Chen, M.; McMurry, P. H.; Smith, J. N. Dependence of Particle Nucleation and Growth on High-Molecular-Weight Gas-Phase Products During Ozonolysis of Alpha-Pinene. *Atmos. Chem. Phys.* **2013**, *13*, 7631−7644.

(18) Moller, K. H.; Berndt, T.; Kjaergaard, H. G. Atmospheric Autoxidation of Amines. *Environ. Sci. Technol.* **2020**, *54*, 11087−11099.

(19) Guenther, A. B.; Jiang, X.; Heald, C. L.; Sakulyanontvittaya, T.; Duhl, T.; Emmons, L. K.; Wang, X. The Model of Emissions of Gases and Aerosols from Nature version 2.1 (MEGAN2.1): An Extended and Updated Framework for Modeling Biogenic Emissions. *Geosci. Model. Dev.* **2012**, *5*, 1471−1492.

(20) Bryant, D. J.; Dixon, W. J.; Hopkins, J. R.; Dunmore, R. E.; Pereira, K.; Shaw, M.; Squires, F. A.; Bannan, T. J.; Mehra, A.; Worrall, S. D.; et al. Strong Anthropogenic Control of Secondary Organic Aerosol Formation from Isoprene in Beijing. *Atmos. Chem. Phys.* **2020**, *20*, 7531−7552.

(21) Riva, M.; Bell, D. M.; Hansen, A. M. K.; Drozd, G. T.; Zhang, Z.; Gold, A.; Imre, D.; Surratt, J. D.; Glasius, M.; Zelenyuk, A. Effect of Organic Coatings, Humidity and Aerosol Acidity on Multiphase Chemistry of Isoprene Epoxydiols. *Environ. Sci. Technol.* **2016**, *50*, 5580−5588.

(22) Heinritzi, M.; Dada, L.; Simon, M.; Stolzenburg, D.; Wagner, A. C.; Fischer, L.; Ahonen, L. R.; Amanatidis, S.; Baalbaki, R.; Baccarini, A.; et al. Molecular Understanding of the Suppression of New-Particle Formation by Isoprene. *Atmos. Chem. Phys.* **2020**, *20*, 11809−11821.

(23) Kroll, J. H.; Ng, N. L.; Murphy, S. M.; Flagan, R. C.; Seinfeld, J. H. Secondary Organic Aerosol Formation from Isoprene Photooxidation. *Environ. Sci. Technol.* **2006**, *40*, 1869−1877.

(24) McFiggans, G.; Mentel, T. F.; Wildt, J.; Pullinen, I.; Kang, S.; Kleist, E.; Schmitt, S.; Springer, M.; Tillmann, R.; Wu, C.; et al. Secondary Organic Aerosol Reduced by Mixture of Atmospheric Vapours. *Nature* **2019**, *565*, 587−593.

(25) Liu, J.; D'Ambro, E. L.; Lee, B. H.; Lopez-Hilfiker, F. D.; Zaveri, R. A.; Rivera-Rios, J. C.; Keutsch, F. N.; Iyer, S.; Kurten, T.; Zhang, Z.; et al. Efficient Isoprene Secondary Organic Aerosol Formation from a Non-IEPDX Pathway. *Environ. Sci. Technol.* **2016**, *50*, 9872−9880.

(26) Berndt, T.; Chen, J.; Kjærgaard, E. R.; Møller, K. H.; Tilgner, A.; Hoffmann, E. H.; Herrmann, H.; Crounse, J. D.; Wennberg, P. O.; Kjaergaard, H. G. Hydrotrioxide (ROOOH) Formation in the Atmosphere. *Science* **2022**, *376*, 979−982.

(27) Lelieveld, J.; Butler, T. M.; Crowley, J. N.; Dillon, T. J.; Fischer, H.; Ganzeveld, L.; Harder, H.; Lawrence, M. G.; Martinez, M.; Taraborrelli, D.; et al. Atmospheric Oxidation Capacity Sustained by a Tropical Forest. *Nature* **2008**, *452*, 737−740.

(28) Liu, Y.; Brito, J.; Dorris, M. R.; Rivera-Rios, J. C.; Seco, R.; Bates, K. H.; Artaxo, P.; Duvoisin, S., Jr.; Keutsch, F. N.; Kim, S.; et al. Isoprene Photochemistry Over the Amazon Rainforest. *Proc. Natl. Acad. Sci. U.S.A.* **2016**, *113*, 6125−6130.

(29) Wells, K. C.; Millet, D. B.; Payne, V. H.; Deventer, M. J.; Bates, K. H.; de Gouw, J. A.; Graus, M.; Warneke, C.; Wisthaler, A.; Fuentes, J. D. Satellite Isoprene Retrievals Constrain Emissions and Atmospheric Oxidation. *Nature* **2020**, *585*, 225−233.

(30) Pierotti, D.; Wofsy, S. C.; Jacob, D.; Rasmussen, R. A. Isoprene and Its Oxidation Products: Methacrolein and Methyl Vinyl Ketone. *J. Geophys. Res. Atmos.* **1990**, *95*, 1871−1881.

(31) Surratt, J. D.; Murphy, S. M.; Kroll, J. H.; Ng, a. L. N.; Hildebrandt, L.; Sorooshian, A.; Szmigielski, R.; Vermeylen, R.; Maenhaut, W.; Claeys, M.; et al. Chemical Composition of Secondary Organic Aerosol Formed from the Photooxidation of Isoprene. *J. Phys. Chem. A* **2006**, *110*, 9665−9690.

(32) Crounse, J. D.; Paulot, F.; Kjaergaard, H. G.; Wennberg, P. O. Peroxy Radical Isomerization in the Oxidation of Isoprene. *Phys. Chem. Chem. Phys.* **2011**, *13*, 13607−13613.

https://doi.org/10.1021/acs.jpca.3c00128
J. Phys. Chem. A 2023, 127, 2819−2829

(33) Canosa-Mas, C. E.; Cotter, E. S. N.; Duffy, J.; Thompson, K. C.; Wayne, R. P. The Reactions of Atomic Chlorine with Acrolein, Methacrolein and Methyl Vinyl Ketone. *Phys. Chem. Chem. Phys.* **2001**, *3*, 3075−3084.
(34) Wang, W. H.; Ezell, M. J.; Ezell, A. A.; Soskin, G.; Finlayson-Pitts, B. J. Rate Constants for the Reactions of Chlorine Atoms with a Series of Unsaturated Aldehydes and Ketones at 298 K: Structure and Reactivity. *Phys. Chem. Chem. Phys.* **2002**, *4*, 1824−1831.
(35) Kaiser, E. W.; Pala, I. R.; Wallington, T. J. Kinetics and Mechanism of the Reaction of Methacrolein with Chlorine Atoms in 1-950 Torr of N_2 or N_2/O_2 Diluent at 297 K. *J. Phys. Chem. A* **2010**, *114*, 6850−6860.
(36) Sun, C.; Xu, B.; Zhang, S. Atmospheric Reaction of Cl + Methacrolein: A Theoretical Study on the Mechanism, and Pressure- and Temperature-Dependent Rate Constants. *J. Phys. Chem. A* **2014**, *118*, 3541−3551.
(37) Aschmann, S. M.; Arey, J.; Atkinson, R. OH Radical Formation from the Gas-Phase Reactions of O_3 with Methacrolein and Methyl Vinyl Ketone. *Atmos. Environ.* **1996**, *30*, 2939−2943.
(38) Deng, J. G.; Chen, J. H.; Geng, C. M.; Liu, H. J.; Wang, W.; Bai, Z. P.; Xu, Y. S. The Overall Reaction Process of Ozone with Methacrolein and Isoprene in the Condensed Phase. *J. Phys. Chem. A* **2012**, *116*, 1710−1716.
(39) Iannone, R.; Koppmann, R.; Rudolph, J. The Stable-Carbon Kinetic Isotope Effects of the Reactions of Isoprene, Methacrolein, and Methyl Vinyl Ketone with Ozone in the Gas Phase. *Atmos. Environ.* **2008**, *42*, 8728−8737.
(40) Tuazon, E. C.; Atkinson, R. A Product Study of the Gas-Phase Reaction of Methacrolein with the OH Radical in the Presence of NO_X. *Int. J. Chem. Kinet.* **1990**, *22*, 591−602.
(41) Gierczak, T.; Burkholder, J. B.; Talukdar, R. K.; Mellouki, A.; Barone, S. B.; Ravishankara, A. R. Atmospheric Fate of Methyl Vinyl Ketone and Methacrolein. *J. Photochem. Photobiol. A* **1997**, *110*, 1−10.
(42) Crounse, J. D.; Knap, H. C.; Ørnsø, K. B.; Jørgensen, S.; Paulot, F.; Kjaergaard, H. G.; Wennberg, P. O. Atmospheric Fate of Methacrolein. 1. Peroxy Radical Isomerization Following Addition of OH and O_2. *J. Phys. Chem. A* **2012**, *116*, 5756−5762.
(43) Zhang, X.; Chen, Z. M.; Zhao, Y. Laboratory Simulation for the Aqueous OH-Oxidation of Methyl Vinyl Ketone and Methacrolein: Significance to the In-Cloud SOA Production. *Atmos. Chem. Phys.* **2010**, *10*, 9551−9561.
(44) Galloway, M. M.; Huisman, A. J.; Yee, L. D.; Chan, A. W. H.; Loza, C. L.; Seinfeld, J. H.; Keutsch, F. N. Yields of Oxidized Volatile Organic Compounds During the OH Radical Initiated Oxidation of Isoprene, Methyl Vinyl Ketone, and Methacrolein under High-NOx Conditions. *Atmos. Chem. Phys.* **2011**, *11*, 10779−10790.
(45) Iannone, R.; Koppmann, R.; Rudolph, J. 12C/13C kinetic isotope effects of the gas-phase reactions of isoprene, methacrolein, and methyl vinyl ketone with OH radicals. *Atmos. Environ.* **2009**, *43*, 3103−3110.
(46) Kwok, E. S. C.; Aschmann, S. M.; Arey, J.; Atkinson, R. Product Formation from the Reaction of the NO_3 Radical with Isoprene and Rate Constants for the Reactions of Methacrolein and Methyl Vinyl Ketone with the NO_3 Radical. *Int. J. Chem. Kinet.* **1996**, *28*, 925−934.
(47) Canosa-Mas, C. E.; Carr, S.; King, M. D.; Shallcross, D. E.; Thompson, K. C.; Wayne, R. P. A Kinetic Study of the Reactions of NO_3 with Methyl Vinyl Ketone, Methacrolein, Acrolein, Methyl Acrylate and Methyl Methacrylate. *Phys. Chem. Chem. Phys.* **1999**, *1*, 4195−4202.
(48) Lin, Y. H.; Zhang, H.; Pye, H. O. T.; Zhang, Z.; Marth, W. J.; Park, S.; Arashiro, M.; Cui, T.; Budisulistiorini, H.; Sexton, K. G.; et al. Epoxide as a Precursor to Secondary Organic Aerosol Formation from Isoprene Photooxidation in the Presence of Nitrogen Oxides. *Proc. Natl. Acad. Sci. U.S.A.* **2013**, *110*, 6718−6723.
(49) Hallquist, M.; Wenger, J. C.; Baltensperger, U.; Rudich, Y.; Simpson, D.; Claeys, M.; Dommen, J.; Donahue, N. M.; George, C.; Goldstein, A. H.; et al. The Formation, Properties and Impact of Secondary Organic Aerosol: Current and Emerging Issues. *Atmos. Chem. Phys.* **2009**, *9*, 5155−5236.
(50) Ma, F.; Guo, X.; Xia, D.; Xie, H. B.; Wang, Y.; Elm, J.; Chen, J.; Niu, J. Atmospheric Chemistry of Allylic Radicals from Isoprene: A Successive Cyclization-Driven Autoxidation Mechanism. *Environ. Sci. Technol.* **2021**, *55*, 4399−4409.
(51) Thornton, J. A.; Kercher, J. P.; Riedel, T. P.; Wagner, N. L.; Cozic, J.; Holloway, J. S.; Dubé, W. P.; Wolfe, G. M.; Quinn, P. K.; Middlebrook, A. M.; et al. A Large Atomic Chlorine Source Inferred from Mid-Continental Reactive Nitrogen Chemistry. *Nature* **2010**, *464*, 271−274.
(52) Tian, L. Molcus Program. http://www.keinsci.com/research/molclus.html (accessed 12/14).
(53) Frisch, M. J.; Trucks, G. W.; Schlegel, H. B.; Scuseria, G. E.; Robb, M. A.; Cheeseman, J. R.; Scalmani, G.; Barone, V.; Mennucci, B.; Petersson, G. A.; et al. *Gaussian 09, Revision A.02*; Inc.: Wallingford: CT, 2009.
(54) Zhao, Y.; Truhlar, D. G. The M06 Suite of Density Functionals for Main Group Thermochemistry, Thermochemical Kinetics, Noncovalent Interactions, Excited States, and Transition Elements: Two New Functionals and Systematic Testing of Four M06-Class Functionals and 12 Other Functionals. *Theor. Chem. Acc.* **2008**, *120*, 215−241.
(55) Benighaus, T.; DiStasio, R. A., Jr.; Lochan, R. C.; Chai, J.-D.; Head-Gordon, M. Semiempirical Double-Hybrid Density Functional with Improved Description of Long-Range Correlation. *J. Phys. Chem. A* **2008**, *112*, 2702−2712.
(56) Glowacki, D. R.; Liang, C. H.; Morley, C.; Pilling, M. J.; Robertson, S. H. MESMER: An Open-Source Master Equation Solver for Multi-Energy Well Reactions. *J. Phys. Chem. A* **2012**, *116*, 9545−9560.
(57) Gilbert, R. G.; Smith, S. C. *Theory of Unimolecular and Recombination Reactions*; Blackwell Scientific: Carlton, Australia, 1990.
(58) Eckart, C. The Penetration of a Potential Barrier by Electrons. *Phys. Rev.* **1930**, *35*, 1303−1309.
(59) Rissanen, M. P.; Eskola, A. J.; Nguyen, T. L.; Barker, J. R.; Liu, J.; Liu, J.; Halme, E.; Timonen, R. S. $CH_2NH_2 + O_2$ and $CH_3CHNH_2 + O_2$ Reaction Kinetics: Photoionization Mass Spectrometry Experiments and Master Equation Calculations. *J. Phys. Chem. A* **2014**, *118*, 2176−2186.
(60) Miller, A. M.; Yeung, L. Y.; Kiep, A. C.; Elrod, M. J. Overall Rate Constant Measurements of the Reactions of Alkene-Derived Hydroxyalkylperoxy Radicals with Nitric Oxide. *Phys. Chem. Chem. Phys.* **2004**, *6*, 3402−3407.
(61) Orlando, J. J.; Tyndall, G. S. Laboratory Studies of Organic Peroxy Radical Chemistry: An Overview with Emphasis on Recent Issues of Atmospheric Significance. *Chem. Soc. Rev.* **2012**, *41*, 6294−6317.
(62) Saunders, S. M.; Jenkin, M. E.; Derwent, R. G.; Pilling, M. J. Protocol for the Development of the Master Chemical Mechanism, MCM v3 (Part A): Tropospheric Degradation of Non-Aromatic Volatile Organic Compounds. *Atmos. Chem. Phys.* **2003**, *3*, 161−180.
(63) Hofzumahaus, A.; Rohrer, F.; Lu, K.; Bohn, B.; Brauers, T.; Chang, C. C.; Fuchs, H.; Holland, F.; Kita, K.; Kondo, Y.; et al. Amplified Trace Gas Removal in the Troposphere. *Science* **2009**, *324*, 1702−1704.
(64) Newland, M. J.; Bryant, D. J.; Dunmore, R. E.; Bannan, T. J.; Acton, W. J. F.; Langford, B.; Hopkins, J. R.; Squires, F. A.; Dixon, W.; Drysdale, W. S.; et al. Low-NO Atmospheric Oxidation Pathways in a Polluted Megacity. *Atmos. Chem. Phys.* **2021**, *21*, 1613−1625.
(65) Atkinson, R.; Arey, J. Atmospheric Degradation of Volatile Organic Compounds. *Chem. Rev.* **2003**, *103*, 4605−4638.
(66) Boyd, A. A.; Flaud, P. M.; Daugey, N.; Lesclaux, R. Rate Constants for $RO_2 + HO_2$ Reactions Measured under a Large Excess of HO_2. *J. Phys. Chem. A* **2003**, *107*, 818−821.
(67) Fang, W. Z.; Gong, L.; Zhang, Q.; Cao, M. Q.; Li, Y.; Sheng, L. S. Measurements of Secondary Organic Aerosol Formed from OH-initiated Photo-oxidation of Isoprene Using Online Photoionization Aerosol Mass Spectrometry. *Environ. Sci. Technol.* **2012**, *46*, 3898−3904.

https://doi.org/10.1021/acs.jpca.3c00128
J. Phys. Chem. A 2023, 127, 2819−2829

(68) Ruppert, L.; Heinz Becker, K. H. A Product Study of the OH Radical-Initiated Oxidation of Isoprene: Formation of C_5-Unsaturated Diols. *Atmos. Environ.* **2000**, *34*, 1529−1542.
(69) Vereecken, L.; Peeters, J. Decomposition of Substituted Alkoxy Radicals-Part I: a Generalized Structure-Activity Relationship for Reaction Barrier Heights. *Phys. Chem. Chem. Phys.* **2009**, *11*, 9062−9074.
(70) Vereecken, L.; Peeters, J. A Structure-Activity Aelationship for the Rate Coefficient of H-Migration in Substituted Alkoxy Radicals. *Phys. Chem. Chem. Phys.* **2010**, *12*, 12608−12620.
(71) Guo, X.; Ma, F.; Liu, C.; Niu, J.; He, N.; Chen, J.; Xie, H. B. Atmospheric Oxidation Mechanism and Kinetics of Isoprene Initiated by Chlorine Radicals: A Computational Study. *Sci. Total Environ.* **2020**, *712*, 136330.

https://doi.org/10.1021/acs.jpca.3c00128
J. Phys. Chem. A 2023, 127, 2819−2829